NANO LETTERS

pubs.acs.org/NanoLett Letter

Electric Field Tunable Ultrafast Interlayer Charge Transfer in Graphene/WS_2 Heterostructure

Yuxiang Liu, Jin Zhang,* Sheng Meng, ChiYung Yam,* and Thomas Frauenheim*

Cite This: *Nano Lett.* 2021, 21, 4403−4409 Read Online

ACCESS | Metrics & More | Article Recommendations | Supporting Information

ABSTRACT: Van der Waals heterostructures composed of two-dimensional materials offer an unprecedented control over their properties and have attracted tremendous research interest in various optoelectronic applications. Here, we study the photo-induced charge transfer in graphene/WS_2 heterostructure by time-dependent density functional theory molecular dynamics. Our results show that holes transfer from graphene to WS_2 two times faster than electrons, and the occurrence of interlayer charge transfer is found correlated with vibrational modes of graphene and WS_2. It is further demonstrated that the carrier dynamics can be efficiently modulated by external electric fields. Detailed analysis confirms that the carrier transfer rate at heterointerface is governed by the coupling between donor and acceptor states, which is the result of the competition between interlayer and intralayer relaxation processes. Our study provides insights into the understanding of ultrafast interlayer charge transfer processes in heterostructures and broadens their future applications in photovoltaic devices.

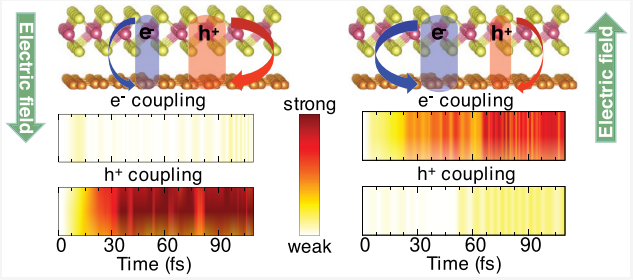

KEYWORDS: *vdW heterostructure, ultrafast charge transfer, electronic coupling, vibrational modes, field modulation*

Van der Waals(vdW) heterostructure are emerging platforms for investigating the concept and design of functional heterostructures for applications in the areas of electronics, photonics, renewable energies, and so forth.[1,2] The newly developed graphene/transition metal dichalcogenides (TMDCs) heterostructure with superior light-absorption properties of TMDCs[3] and high electrical conductivity of graphene[4,5] has been taken as potential materials for novel optoelectronic devices.[6−8] This drives many experimental and theoretical studies focusing on the ultrafast charge transfer process at graphene/TMDCs heterointerfaces.[9−15] For instance, it has been shown that photoinduced interlayer electron transfer takes place within 1 ps in graphene/$MoSe_2$ heterostructure.[16] Similar results are reported in graphene/WS_2 heterostructure, where the transfer of photoexcited holes takes less than 200 fs, an order of magnitude faster than that of electrons.[17−19] However, the origin of ultrafast interlayer charge transfer in weak coulping graphene/TMDCs heterostructures is still unclear.

From the perspective of practical applications, electric fields have been taken as one of the most effective approaches to manipulate the electronic and optical properties of TMDCs due to their nondestructive and reversible nature.[20−22] For example, electric field tunable electrical and optical properties have been demonstrated in graphene/WSe_2 heterostructures.[23] For optoelectronics, it has been shown that an external electric field can be used to modulate the amplitude and even reverse the polarity of photocurrent in graphene/MoS_2/graphene devices.[24] Similarly, the gate-tunable photocurrent is also demonstrated in graphene/WS_2/graphene devices.[25] As a photodetector, graphene/WS_2/graphene stack has shown to exhibit outstanding photoresponse, which is achieved by the modulation of the Schottky barriers between graphene and WS_2 with a gate voltage.[26] Although many experimental efforts have been made to study the device properties of different graphene/TMDCs heterostructures, the detailed mechanism of the microscopic processes remain uncertain.

In this work, we utilize time-dependent density functional theory (TDDFT) combined with nonadiabatic molecular dynamics (NAMD) to investigate the ultrafast charge transfer in a graphene/WS_2 heterostructure. Our results demonstrate that photoexcited holes transfer from WS_2 to graphene more efficiently than electrons. The ultrafast charge transfer arises from the coupling to the nuclear vibrations of graphene and WS_2 and its amplitude and polarity show a strong dependence on the external electric fields. Further analysis reveals that the interlayer charge transfer process in graphene/WS_2 heterostructure is governed by the coupling between carriers and the final states; in other words, it is the result of competition between carrier interlayer and intralayer relaxation processes.

Received: March 17, 2021
Revised: May 9, 2021
Published: May 17, 2021

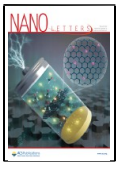

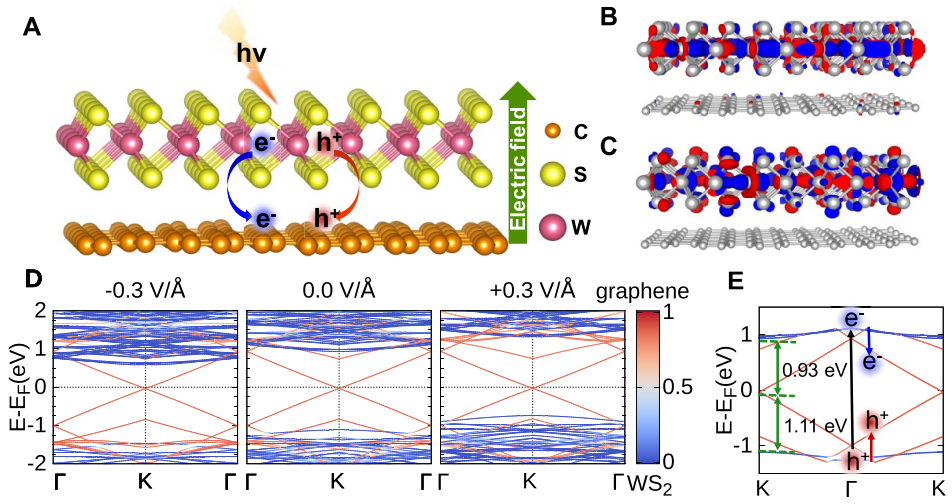

Figure 1. Electronic structures of graphene/WS_2 heterostructure. (A) Illustration of the graphene/WS_2 heterostructure, where WS_2 lies on top of graphene. Holes and electrons excited by incident light transfer from WS_2 to graphene layer. The brown, yellow, and purple spheres represent carbon, sulfur, and tungsten atoms, respectively. The green arrow represents positive electric field direction, pointing from graphene to WS_2. Wave function of (B) VBM and (C) CBM states of WS_2 on Γ-point, positive and negative parts are in red and blue, respectively. The same crystal structure as panel A is employed. To highlight the wave function, all atoms are represented by gray spheres. (D) The band structures of the heterostructure with different external electric fields varying from −0.3 to +0.3 V/Å. E_F are set to zero. The color of each band indicates the degree of localization of each state to graphene and WS_2, where one (red) represents that the state completely localizes to graphene, while zero (blue) represents that the state completely localizes to WS_2. (E) Band structures in the vicinity of Γ-point with zero external field to illustrate the photoexcitation process. Incident light excites one electron from the VBM of WS_2 to its CBM, as indicated by the black arrow. The photoexcited hole and electron are then transferred to nearby graphene states, as indicated by red and blue arrows, respectively. The color map is the same as in panel D.

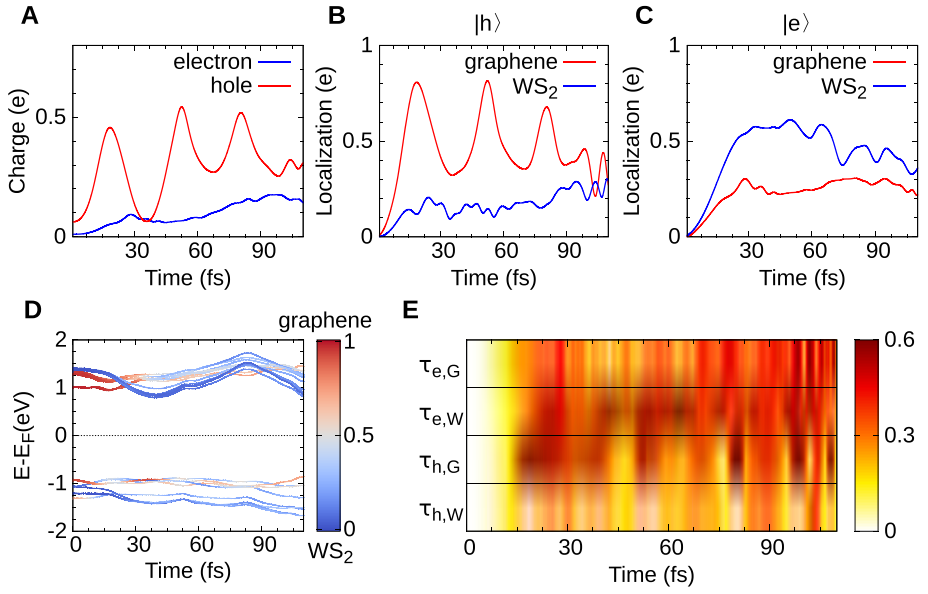

Figure 2. Excitation dynamics of graphene/WS_2 heterostructure. (A) Amount of photoexcited hole and electron transferred from WS_2 to graphene. The electron and hole transfer are shown in blue and red, respectively as a function of time. Time evolution of photoexcited (B) hole and (C) electron localization $\gamma_{e/h}(t)$ on graphene and WS_2 layers. (D) Time evolution of energy levels $\epsilon(t)$. Same color map as in Figure 1D is employed to show the charge localization. (E) Time evolution of the couplings, $\tau_{e,G}(t)$, $\tau_{e,W}(t)$, $\tau_{h,G}(t)$, and $\tau_{h,W}(t)$. The color indicates the strength of the coupling between photoexcited carriers and acceptor states.

We show that nuclear vibrations in graphene and WS_2 enhance the interlayer couplings and facilitate interlayer charge transfer. This work establishes a firm correlation between the charge dynamics and couplings between states in 2D heterostructures and thus paves the way for their future applications in optoelectronics.

The electron and nuclear dynamics are simulated within the time-dependent ab initio package (TDAP).[27] More computational details are presented in Supporting Information. To investigate the photoinduced charge transfer process at the graphene/WS_2 interface, we built an atomic model shown in Figure 1A. The system is initially in the ground state and it is assumed that an electron−hole pair is generated in WS_2 upon photoexcitation at the beginning of the time evolution. Specifically, an electron is removed from an occupied state and placed in an empty state that are both localized within

https://doi.org/10.1021/acs.nanolett.1c01083
Nano Lett. 2021, 21, 4403−4409

WS_2. Because of the weak vdW interaction, the electronic structure is essentially a superposition of individual band structures of graphene and WS_2. In the heterostructure, the Dirac point of graphene is located ~34 meV below the Fermi level (E_F) with a negligible band gap of 4.3 meV. On the other hand, WS_2 remains a direct semiconductor with a band gap of 2.04 eV at K point. As shown in Figure 1E, the valence band maximum (VBM) of WS_2 is located 1.11 eV below E_F and the conduction band minimum (CBM) is located 0.93 eV above E_F. Our calculations are consistent with angle-resolved photoemission spectroscopy measurements, where the VBM of WS_2 is located 1.2 eV below E_F.[17] The wave function also indicates that the weak vdW interaction indeed has a minor effect on the electronic structures (Figure 1B,C), where VBM and CBM states of WS_2 are localized almost entirely to itself. The microscopic processes upon photoexcitation are shown in Figure 1E, optical absorption in the graphene/WS_2 heterostructure results in a direct excitation of electrons from VBM to CBM of WS_2, and consequently holes and electrons transfer to the nearby graphene states. We denote the local WS_2 VBM and CBM where the photoexcited carriers are located by $|h\rangle$ and $|e\rangle$, respectively.

To visualize the charge transfer process, time evolution of photoinduced carriers is followed, as plotted in Figure 2A. The amount of carriers in $|h\rangle$ and $|e\rangle$ transferred from WS_2 to graphene is calculated by integrating the carrier density over the whole graphene layer

$$n_i(t) = \sum_{\mu,\nu\epsilon\text{graphene}} c^*_{\mu i}(t) S_{\mu\nu}(t) c_{\nu i}(t) \tag{1}$$

where c is the molecular orbital coefficient, and S is the overlap matrix. μ, ν are the atomic orbitals that belong to graphene, and i represents $|h\rangle$ or $|e\rangle$.

Obviously, $n_h(t)$ oscillates by periodically filling and emptying graphene states at a period of ~35 fs, and a gradual accumulation of ~0.30 hole on the graphene layer is observed within 100 fs. Meanwhile, $n_e(t)$ shows a relatively slow and steadily increasing trend with about ~0.15 electron transferring to graphene layer. Our calculations are in accordance with results attained via transient reflection measurements and time-resolved photoemission spectroscopy, in which transfer of light-induced holes to graphene is more efficient than that of electrons with a lifetime of ~200 fs and ~1 ps for hole and electron, respectively.[9,19] Aeschlimann et al. attributed this difference to the energetic alignment of the heterostructure, in which p-doped graphene has ~6 times higher density of states available for hole transfer as compared to that for electron transfer.[17] However, in this work, pristine graphene is employed and the density of acceptor states for electrons and holes are similar, as shown in Figure S1. As shown in Figure 2D, the energies of acceptor states on graphene locate between $\epsilon_h(t)$ and $\epsilon_e(t)$. As the system evolves, both $|h\rangle$ and $|e\rangle$ get closer to their acceptor states. Consequently, $|h\rangle$ and acceptor states on graphene overlap at ~15 fs while this only happens at a later time ~25 fs for $|e\rangle$. The overlap of energy states enhances the coupling between donor and acceptor states, resulting in an ultrafast charge transfer to graphene. On the basis of our simulation results, the faster interlayer hole transfer can be attributed to the stronger coupling. For further investigation, we quantify the coupling between the donor and acceptor states by projecting the time-dependent density matrix onto initial eigenstates (more details are presented in Supporting Information).

$$\sigma_{ij}(t) = \sum_{\mu\nu\kappa\lambda} (c_{\mu i}(0) S_{\kappa\mu})^* P_{\kappa\lambda}(t) S_{\lambda\nu} c_{\nu j}(0) \tag{2}$$

where P is the single-electron density matrix. The coupling is then obtained by summing up all the states from $|h-5\rangle$ to $|e+5\rangle$ within the layer of interest.

$$\tau_{i,L}(t) = \sum_{j\neq i, j=h-5}^{e+5} |\sigma_{ij}(t)| \tag{3}$$

where L corresponds to either graphene (G) or WS_2 (W) and i is $|h\rangle$ or $|e\rangle$.

As shown in Figure 2E, $|h\rangle$ couples stronger to the states on graphene while $|e\rangle$ couples stronger to the states on WS_2. Precisely, the time averaged value of $\tau_{h,G}(t)$ is ~0.27, which is twice as large as that of $\tau_{h,W}(t)$ (~0.14). This is consistent with the tunneling model founded by Krause et al. They demonstrated that interlayer charge transfer is determined by the direct tunneling at points in Brillouin zone where WS_2 and graphene band cross, while the tunneling matrix element for hole is much larger than that for electron.[18] Thus, despite the weak binding of the heterostructure, photoexcited hole interlayer transfer occurs at an ultrafast time scale. On the other hand, intralayer relaxation within WS_2 are more efficient for the photoexcited electron. These results can be further demonstrated by defining the charge localization

$$\gamma_h(t) = \sum_{j\neq h, j=h-5}^{e+5} |\langle j(0)|h(t)\rangle|^2, \quad \gamma_e(t) = \sum_{j\neq e, j=h-5}^{e+5} |\langle j(0)|e(t)\rangle|^2 \tag{4}$$

Consistently with our previous results, Figure 2B,C shows that the excited hole delocalized more rapidly to graphene due to the strong coupling $\tau_{h,G}(t)$. In the case of the excited electron, a large proportion remains localized on the WS_2 layer due to the more efficient intralayer relaxation. Thus, there is a competition between carrier interlayer and intralayer relaxation which can be determined by the coupling $\tau_{e/h,L}(t)$. Next, we investigate how the charge dynamics in the graphene/TMDCs heterostructures is influenced by the nuclear degrees of freedom.

To reveal the relationship between the interlayer carrier dynamics and nuclear vibrational modes, Fourier transforms (FTs) of dynamics of $n_{e/h}(t)$, $\epsilon_{e/h}(t)$, and $\tau_{e/h,G}(t)$ are performed. As shown in Figure 3A, the hole transfer $n_h(t)$ displays characteristic frequencies at ~1067 and ~1584 cm^{-1}. The oscillation at ~1067 cm^{-1} can also be found in the FTs of $\epsilon_h(t)$ as highlighted in the gray shaded area of Figure 3A. This frequency however does not match any vibrational mode of either graphene or WS_2, and the origin of this oscillation component will be discussed later. The ~1584 cm^{-1} oscillation (Figure 3A, red shaded area) reflects the excitation of the C=C stretching mode G,[28] which can also be observed in the dynamics of $n_e(t)$ (Figure 3B, red shaded area). In the case of electron dynamics, apart from G mode, a noticeable peak at ~413 cm^{-1} (Figure 3B, left red shaded area) is found in FTs of $\epsilon_e(t)$ and $\tau_{e,G}(t)$, reflecting an out-of-plane vibrational mode A_{1g} of sulfur atoms in the WS_2 layer.[29] On the other hand, the oscillatory components at ~620 cm^{-1} (Figure 3B, gray shaded area) are not associated with any vibrational modes of graphene or WS_2. Therefore, it is expected that the C=C stretching mode G should be responsible for both interlayer electron and hole transfer processes while the out-of-plane vibrational mode A_{1g} should instead associated with the electron transfer only.

https://doi.org/10.1021/acs.nanolett.1c01083
Nano Lett. 2021, 21, 4403−4409

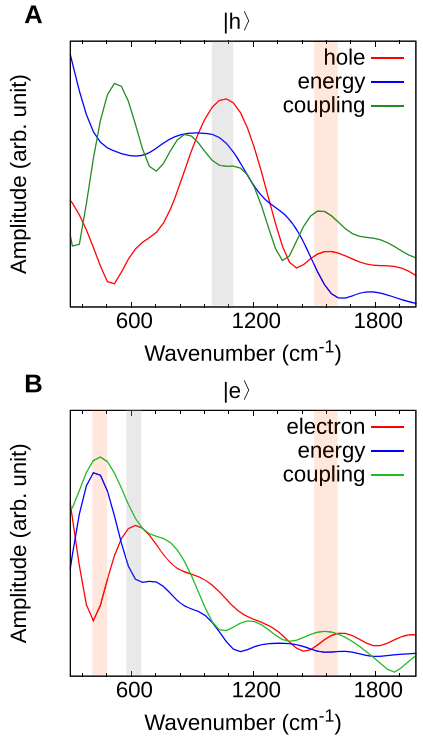

Figure 3. Comparison of FTs of photoexcited (A) hole and (B) electron transferred to graphene $n_{e/h}(t)$, their corresponding energies $\epsilon_{e/h}(t)$ and the couplings to electronic states of graphene layer $\tau_{e/h,G}(t)$. Red, blue, and green curves correspond to the FTs of $n_{e/h}(t)$, $\epsilon_{e/h}(t)$, and $\tau_{e/h,G}(t)$, respectively. The red shaded areas highlight the frequencies associated with ionic vibrations, and the gray shaded areas represent the frequencies associated with the collective motion of carriers.

To better understand the role of nuclear vibrational modes in the interlayer charge transfer processes and verify our statement, the scenarios of fixed ionic motions are investigated. We decouple the ionic motion from the charge dynamics by freezing atoms (i) in both layers, (ii) in WS_2 only, and (iii) in graphene only, and excitation dynamics is shown in Figure 4. With all of the ions clamped, the charge dynamics $n_i(t)$ presents two main features: (i) For photoexcited hole, a periodic sloshing between WS_2 and graphene with a prominent amplitude is observed, but there is no net transfer within the simulation period. (ii) The electron dynamics is totally suppressed. These results further demonstrate that couplings between graphene electronic and nuclear degrees of freedom are responsible for the interlayer charge transfer in the graphene/WS_2 heterostructure, in which the energy of carriers is dissipated to nuclear motions during the transition. Figure S3 shows that excited electron and hole dynamics both exhibit a distinct oscillation at ∼657 and ∼1100 cm^{-1}, which is consistent with the above frequencies at ∼620 and ∼1067 cm^{-1} in the case of moving atoms. This is the same as that in MoS_2/WS_2 heterostructure, where hole dynamics present a similar oscillation when all of the atoms are clamped. Wang et al. demonstrated that the origin of coherent oscillation is the result of collective motion of holes, which lead to strong dynamic coupling due to the electric field caused by charge transfer.[30] Therefore, the characteristic oscillation of charge dynamics comes from the collective motion of carriers. From Figure 4C, there is essentially no coupling between the graphene acceptor states and the photoexcited electron with a time-averaged value of 0.01. Instead, |e⟩ couples more strongly to the WS_2 states with a time-averaged value of 0.32. As a result, a majority of photoexcited electron resides on the WS_2 but relaxes to neighboring WS_2 states (Figure S4B).

We further investigate the scenario when only the atoms in WS_2 layer are clamped. Similarly, the photoexcited hole fills and empties periodically the nearby graphene states with a net amount of 0.2 transferred to the graphene layer after 100 fs. Meanwhile, the photoexcited electron gradually builds up in the graphene layer with a value of 0.1 within the same period. This carrier transfer rate is reduced by as much as half compared to the case with moving atoms. In the case of frozen graphene, electron dynamics shows a similar trend as fixed WS_2, but no net hole transfer is observed within 100 fs. The FTs results show that electron and hole dynamics both display the characteristic frequency of G-mode with fixed WS_2, while A_{1g}-mode oscillation only shows in electron dynamics with fixed graphene (Figure S5). Meanwhile, Figure 1B,C indcate that |e⟩ distributes over the whole sandwich structure of WS_2 while |h⟩ is largely localized on W atoms. These results imply that the vibration of graphene is associated with electron and hole interlayer transfer process while the vibration of WS_2 only contributes to electron interlayer dynamics.

Currently, intensive experimental studies focus on highly efficient electric field tunable interlayer charge relaxations in graphene/TMDCs heterostructures. It was reported that the built-in potential induced by gate-tunable Schottky barrier can accelerate interlayer charge transfer in graphene/MoS_2, achieving the modulation of amplitude and polarity of photocurrent.[24] The same photocurrent response was found in graphene/WSe_2.[23] As aforementioned, the observed ultrafast interlayer charge transfer is the result of competition between interlayer and intralayer relaxation which is determined by the corresponding coupling. Thus, understanding how $\tau_{e/h,L}(t)$ can be controlled by external fields is a key to manipulate charge dynamics. We apply vertical external electric fields to the heterostructure with strengths varying from −0.3 to +0.3 V/Å. Figure 1D shows that applied electric field has a negligible effect on the electronic properties of graphene but shifts the energy states of WS_2. With a −0.3 V/Å electric field, WS_2 states are downshifted by 0.4 eV. As shown in Figure S1, negative electric field increases the density of acceptor states for hole while decrease the density for electron. On the contrary, a +0.3 V/Å electric field upshifts the WS_2 energy states by 0.4 eV and thus facilitates the electron transfer and suppressed the hole transfer. Figure 5A shows that the negative electric field indeed facilitates interlayer hole transfer and ∼0.35 of hole is transferred to graphene layer within 100 fs, which is faster than the case without electric field. Meanwhile interlayer electron transfer is completely impeded. Contrary to this, positive electric field accelerates electron transfer with ∼0.25 excited electron delocalized to graphene after 100 fs, compared to the amount of ∼0.15 in the case without electric field. These results are consistent with experimental observations in graphene/MoS_2/graphene heterostructure, where applied with a −6 V top-gate bias accelerates photoexcited hole transfer to top graphene while a +4 V bias modulates the polarity of photocurrent by motivating electron transfer to graphene.[24] The scenarios with ±0.1 V/Å applied fields are presented in Figures S6 and S7 in which the charge dynamics exhibits a similar response to the external electric fields.

To further explore the origin of an electric field tunable interlayer relaxation process, we present the time evolution of

https://doi.org/10.1021/acs.nanolett.1c01083
Nano Lett. 2021, 21, 4403−4409

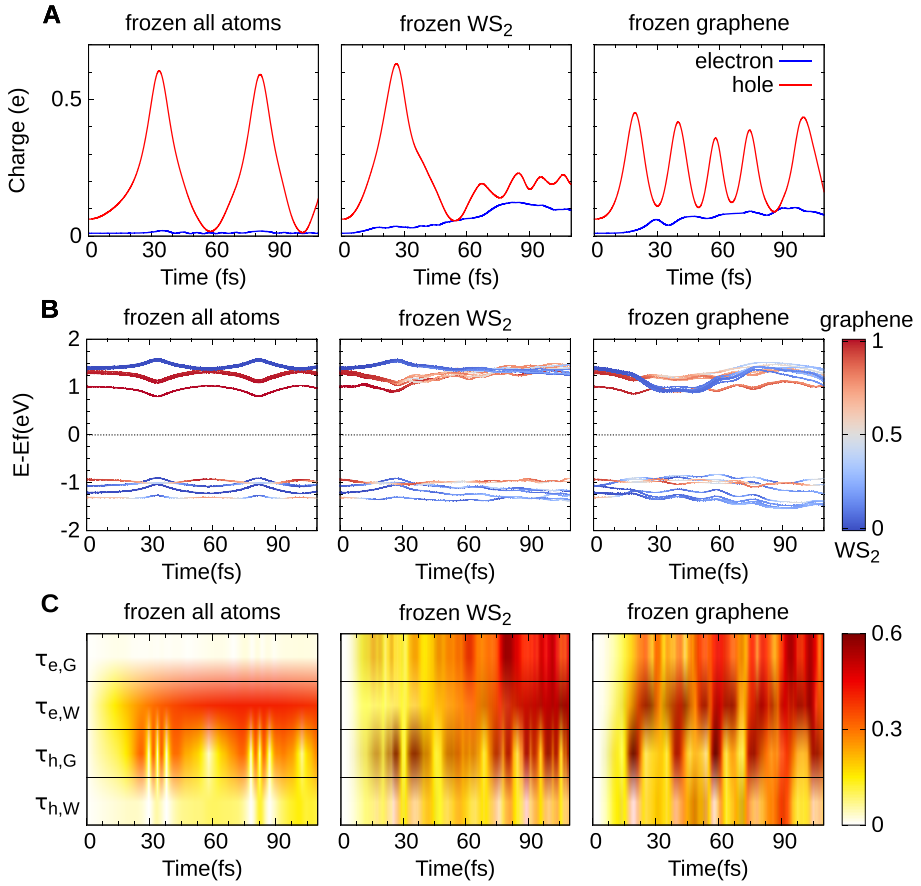

Figure 4. Excitation dynamics of graphene/WS_2 heterostructure with all frozen atoms, frozen WS_2 layer, and frozen graphene layer. (A) Amount of photoexcited electron and hole transferred from WS_2 to graphene. (B) Time evolution of the energy levels $\epsilon(t)$. The same color map as the Figure 1D is employed to show the charge localization. (C) Time evolution of the couplings, $\tau_{e,G}(t)$, $\tau_{e,W}(t)$, $\tau_{h,G}(t)$ and $\tau_{h,W}(t)$. The color indicates the strength of the coupling between photoexcited carriers and acceptor states.

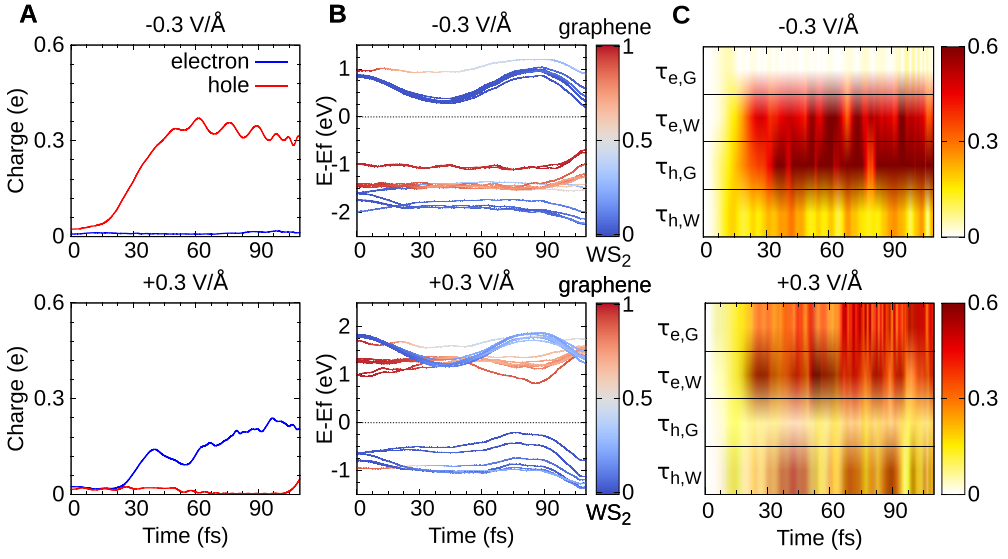

Figure 5. Excitation dynamics of graphene/WS_2 heterostructure with external electric fields varying from −0.3 to +0.3 V/Å. (A) Amount of photoexcited electron and hole transferred from WS_2 to graphene. (B) Time evolution of the energy levels $\epsilon(t)$. Same color map as the Figure 1D is employed to show the charge localization. (C) Time evolution of the couplings, $\tau_{e,G}(t)$, $\tau_{e,W}(t)$, $\tau_{h,G}(t)$ and $\tau_{h,W}(t)$. The color indicates the strength of the coupling between photoexcited carriers and acceptor states.

energy levels and corresponding couplings in Figure 5B,C. Since a negative electric field introduces a higher density of acceptor states available for hole transfer, $\tau_{h,G}(t)$ is enhanced as $|h\rangle$ evolves and significantly accelerates the hole transfer. On the contrary, the positive electric field has the same effect on electron and thus stronger $\tau_{e,G}(t)$ facilitates the interlayer

https://doi.org/10.1021/acs.nanolett.1c01083
Nano Lett. 2021, 21, 4403−4409

electron transfer. Comparing the couplings in Figure 5C with that in Figure 2E, the applied electric field indeed has significant effects on the coupling between donor and acceptor states and hence the charge transfer rate. Thus, by applying electric field perpendicular to the heterostructure, it it possible to accelerate or slow down interlayer charge transfer selectively and therefore aid the separation of photogenerated carriers. This offers a versatile method to control the photoinduced carrier generation, separation, and transport process in graphene/TMDCs heterostructures.

Ehrenfest dynamics, for long simulation time, results in mean vibrational energies that exceed the thermodynamical limit.[31,32] As such, the TDDFT simulations are expected to overestimate vibronic coherence phenomena and underestimate dephasing. Therefore, careful benchmark to time-resolved experiments and higher level quantum dynamics simulations, for example, multiconfiguration time-dependent Hartree (MCTDH) methods, is warranted. On the other hand, there are existing methods which add decoherence in Ehrenfest dynamics to improve the accuracy of predicted time scales.[33−35] These approaches will be explored in our future work for quantitative studies. Meanwhile, it is well-known that PBE functional suffers from delocalization error and this results in too low energy for delocalized densities. One common remedy is to incorporate fraction of Hartree−Fock exchange in the exchange-correlation functional. In this work, we mainly focus on the difference between charge transfer rates of excited electrons and holes. Thus, we expect the main conclusion of faster hole transfer from graphene to WS_2 would remain the same despite of the delocalization error.

In summary, we employ the ab initial TDDFT-NAMD method to investigate the ultrafast interlayer charge transfer process in graphene/WS_2 heterostructure. Our study reveals that interlayer charge transfer process is mainly determined by the coupling between photoexcited carriers and acceptor states on graphene. This explains the different transfer rates of excited carriers in graphene/WS_2 heterostructure and it is expected our findings can be applied to other vdW heterostructures. In addition, it is found that nuclear vibrations in graphene and WS_2 can enhance the interlayer couplings and facilitate the charge transfer. Specifically, the C=C stretching mode G is associated with both interlayer electron and hole transfer process while out-of-plane vibrational mode A_{1g} is associated with the electron transfer only. Further, we demonstrate the possibility of electric field modulation of the interlayer couplings and enhance the control of carrier dynamics. On the basis of these findings, one could utilize external electric fields to manipulate the quantum dynamics of excited carriers at heterointerfaces. These results not only provide a deep understanding of interfacial phenomena but also offer new insights for building ultrasensitive optoelectronic devices.

■ ASSOCIATED CONTENT

Supporting Information

The Supporting Information is available free of charge at https://pubs.acs.org/doi/10.1021/acs.nanolett.1c01083.

Details of nonadiabatic molecular dynamics, computational details, electronic structures, vibrational analysis, and charge dynamics with electric fields (PDF)

■ AUTHOR INFORMATION

Corresponding Authors

Jin Zhang − *Center for Free Electron Laser Science, Max Planck Institute for the Structure and Dynamics of Matter, 22761 Hamburg, Germany;* orcid.org/0000-0001-7830-3464; Email: jin.zhang@mpsd.mpg.de

ChiYung Yam − *Beijing Computational Science Research Center, 100193 Beijing, China; Shenzhen JL Computational Science and Applied Research Institute, 518109 Shenzhen, China;* orcid.org/0000-0002-3860-2934; Email: yamcy@csrc.ac.cn

Thomas Frauenheim − *Bremen Center for Computational Materials Science, University of Bremen, 28359 Bremen, Germany; Beijing Computational Science Research Center, 100193 Beijing, China; Shenzhen JL Computational Science and Applied Research Institute, 518109 Shenzhen, China;* Email: thomas.frauenheim@bccms.uni-bremen.de

Authors

Yuxiang Liu − *Bremen Center for Computational Materials Science, University of Bremen, 28359 Bremen, Germany;* orcid.org/0000-0003-3092-3044

Sheng Meng − *Beijing National Laboratory for Condensed Matter Physics and Institute of Physics, Chinese Academy of Sciences, 100190 Beijing, China;* orcid.org/0000-0002-1553-1432

Complete contact information is available at: https://pubs.acs.org/10.1021/acs.nanolett.1c01083

Notes

The authors declare no competing financial interest.

■ ACKNOWLEDGMENTS

The authors acknowledge Agnieszka Kuc for providing the crystal structure of graphene/WS_2 heterostructure and Angel Rubio for helpful discussions. The support from the NSFC (Grants 22073007 and U1930402), the Guangdong Shenzhen Joint Key Fund (Grant 2019B1515120045), the DFG (Grant RTG2247), the Shenzhen Basic Research Fund (Grant JCYJ20190813164805689), the Sino-German Mobility Program (Grant M-0215), the Supercomputer Center of Northern Germany via HLRN (Grant hbp00067), and Hong Kong Quantum AI Lab is gratefully acknowledged. J.Z. acknowledges funding from the European Union Horizon 2020 research and innovation program under Marie Sklodowska-Curie Grant Agreement 886291 (PeSD-NeSL).

■ REFERENCES

(1) Yu, W. J.; Li, Z.; Zhou, H.; Chen, Y.; Wang, Y.; Huang, Y.; Duan, X. Vertically Stacked Multi-Heterostructures of Layered Materials for Logic Transistors and Complementary Inverters. *Nat. Mater.* **2013**, *12*, 246−252.

(2) Jariwala, D.; Sangwan, V. K.; Lauhon, L. J.; Marks, T. J.; Hersam, M. C. Emerging Device Applications for Semiconducting Two-Dimensional Transition Metal Dichalcogenides. *ACS Nano* **2014**, *8*, 1102−1120.

(3) Wang, Q. H.; Kalantar-Zadeh, K.; Kis, A.; Coleman, J. N.; Strano, M. S. Electronics and Optoelectronics of Two-Dimensional Transition Metal Dichalcogenides. *Nat. Nanotechnol.* **2012**, *7*, 699−712.

(4) Novoselov, K. S.; Geim, A. K.; Morozov, S. V.; Jiang, D.; Zhang, Y.; Dubonos, S. V.; Grigorieva, I. V.; Firsov, A. A. Electric Field Effect in Atomically Thin Carbon Films. *Science* **2004**, *306*, 666−669.

(5) Novoselov, K. S.; Geim, A. K.; Morozov, S. V.; Jiang, D.; Katsnelson, M. I.; Grigorieva, I. V.; Dubonos, S. V.; Firsov, A. A. Two-Dimensional Gas of Massless Dirac Fermions in Graphene. *Nature* **2005**, *438*, 197−200.
(6) Georgiou, T.; Jalil, R.; Belle, B. D.; Britnell, L.; Gorbachev, R. V.; Morozov, S. V.; Kim, Y.-J.; Gholinia, A.; Haigh, S. J.; Makarovsky, O.; et al. Vertical Field-Effect Transistor Based on Graphene-WS_2 Heterostructures for Flexible and Transparent Electronics. *Nat. Nanotechnol.* **2013**, *8*, 100.
(7) Liu, X.; Gao, P.; Hu, W.; Yang, J. Photogenerated-Carrier Separation and Transfer in Two-Dimensional Janus Transition Metal Dichalcogenides and Graphene Van Der Waals Sandwich Heterojunction Photovoltaic Cells. *J. Phys. Chem. Lett.* **2020**, *11*, 4070−4079.
(8) Liu, Y.; Weiss, N. O.; Duan, X.; Cheng, H.-C.; Huang, Y.; Duan, X. Van Der Waals Heterostructures and Devices. *Nat. Rev. Mater.* **2016**, *1*, 1−17.
(9) He, J.; Kumar, N.; Bellus, M. Z.; Chiu, H.-Y.; He, D.; Wang, Y.; Zhao, H. Electron Transfer and Coupling in Graphene-Tungsten Disulfide Van Der Waals Heterostructures. *Nat. Commun.* **2014**, *5*, 1−5.
(10) Iida, K.; Noda, M.; Nobusada, K. Photoinduced Electron Transfer at the Interface between Heterogeneous Two-Dimensional Layered Materials. *J. Phys. Chem. C* **2018**, *122*, 21651−21658.
(11) Shan, H.; Yu, Y.; Zhang, R.; Cheng, R.; Zhang, D.; Luo, Y.; Wang, X.; Li, B.; Zu, S.; Lin, F.; et al. Electron Transfer and Cascade Relaxation Dynamics of Graphene Quantum Dots/MoS_2 Monolayer Mixed-Dimensional Van Der Waals Heterostructures. *Mater. Today* **2019**, *24*, 10−16.
(12) Wen, X.; Chen, H.; Wu, T.; Yu, Z.; Yang, Q.; Deng, J.; Liu, Z.; Guo, X.; Guan, J.; Zhang, X. Ultrafast Probes of Electron-Hole Transitions between Two Atomic Layers. *Nat. Commun.* **2018**, *9*, 1−9.
(13) Massicotte, M.; Schmidt, P.; Vialla, F.; Watanabe, K.; Taniguchi, T.; Tielrooij, K.-J.; Koppens, F. H. Photo-Thermionic Effect in Vertical Graphene Heterostructures. *Nat. Commun.* **2016**, *7*, 1−7.
(14) Garcia-Basabe, Y.; Rocha, A. R.; Vicentin, F. C.; Villegas, C. E.; Nascimento, R.; Romani, E. C.; De Oliveira, E. C.; Fechine, G. J.; Li, S.; Eda, G.; et al. Ultrafast Charge Transfer Dynamics Pathways in Two-Dimensional MoS_2-Graphene Heterostructures: a Core-Hole Clock Approach. *Phys. Chem. Chem. Phys.* **2017**, *19*, 29954−29962.
(15) Yuan, L.; Chung, T.-F.; Kuc, A.; Wan, Y.; Xu, Y.; Chen, Y. P.; Heine, T.; Huang, L. Photocarrier Generation from Interlayer Charge-Transfer Transitions in WS_2-Graphene Heterostructures. *Sci. Adv.* **2018**, *4*, e1700324.
(16) Froehlicher, G.; Lorchat, E.; Berciaud, S. Charge Versus Energy Transfer in Atomically Thin Graphene-Transition Metal Dichalcogenide Van Der Waals Heterostructures. *Phys. Rev. X* **2018**, *8*, 011007.
(17) Aeschlimann, S.; Rossi, A.; Chávez-Cervantes, M.; Krause, R.; Arnoldi, B.; Stadtmüller, B.; Aeschlimann, M.; Forti, S.; Fabbri, F.; Coletti, C.; et al. Direct Evidence for Efficient Ultrafast Charge Separation in Epitaxial WS_2/Graphene Heterostructures. *Sci. Adv.* **2020**, *6*, eaay0761.
(18) Krause, R.; Aeschlimann, S.; Chavez-Cervantes, M.; Perea-Causin, R.; Brem, S.; Malic, E.; Forti, S.; Fabbri, F.; Coletti, C.; Gierz, I. Microscopic Understanding of Ultrafast Charge Transfer in Van-Der-Waals Heterostructures. 2020, *arXiv: 2012.09268*, Cond. Mat. Mes. Hall., https://arxiv.org/abs/2012.09268 (accessed Dec. 16, 2020).
(19) He, J.; He, D.; Wang, Y.; Zhao, H. Probing Effect of Electric Field on Photocarrier Transfer in Graphene-WS_2 Van Der Waals Heterostructures. *Opt. Express* **2017**, *25*, 1949−1957.
(20) Jones, A. M.; Yu, H.; Ghimire, N. J.; Wu, S.; Aivazian, G.; Ross, J. S.; Zhao, B.; Yan, J.; Mandrus, D. G.; Xiao, D.; et al. Optical Generation of Excitonic Valley Coherence in Monolayer WSe_2. *Nat. Nanotechnol.* **2013**, *8*, 634−638.
(21) Wu, S.; Ross, J. S.; Liu, G.-B.; Aivazian, G.; Jones, A.; Fei, Z.; Zhu, W.; Xiao, D.; Yao, W.; Cobden, D.; et al. Electrical Tuning of Valley Magnetic Moment Through Symmetry Control in Bilayer MoS_2. *Nat. Phys.* **2013**, *9*, 149−153.
(22) Ramasubramaniam, A.; Naveh, D.; Towe, E. Tunable Band Gaps in Bilayer Transition-Metal Dichalcogenides. *Phys. Rev. B: Condens. Matter Mater. Phys.* **2011**, *84*, 205325.
(23) Li, Y.; Qin, J.-K.; Xu, C.-Y.; Cao, J.; Sun, Z.-Y.; Ma, L.-P.; Hu, P. A.; Ren, W.; Zhen, L. Electric Field Tunable Interlayer Relaxation Process and Interlayer Coupling in WSe_2/Graphene Heterostructures. *Adv. Funct. Mater.* **2016**, *26*, 4319−4328.
(24) Yu, W. J.; Liu, Y.; Zhou, H.; Yin, A.; Li, Z.; Huang, Y.; Duan, X. Highly Efficient Gate-Tunable Photocurrent Generation in Vertical Heterostructures of Layered Materials. *Nat. Nanotechnol.* **2013**, *8*, 952−958.
(25) Britnell, L.; Ribeiro, R.; Eckmann, A.; Jalil, R.; Belle, B.; Mishchenko, A.; Kim, Y.-J.; Gorbachev, R.; Georgiou, T.; Morozov, S.; et al. Strong Light-Matter Interactions in Heterostructures of Atomically Thin Films. *Science* **2013**, *340*, 1311−1314.
(26) Tan, H.; Fan, Y.; Zhou, Y.; Chen, Q.; Xu, W.; Warner, J. H. Ultrathin 2D Photodetectors Utilizing Chemical Vapor Deposition Grown WS_2 with Graphene Electrodes. *ACS Nano* **2016**, *10*, 7866−7873.
(27) Meng, S.; Kaxiras, E. Real-time, Local Basis-Set Implementation of Time-Dependent Density Functional Theory for Excited State Dynamics Simulations. *J. Chem. Phys.* **2008**, *129*, 054110.
(28) Dresselhaus, M. S.; Jorio, A.; Hofmann, M.; Dresselhaus, G.; Saito, R. Perspectives on Carbon Nanotubes and Graphene Raman Spectroscopy. *Nano Lett.* **2010**, *10*, 751−758.
(29) Zhao, W.; Ghorannevis, Z.; Amara, K. K.; Pang, J. R.; Toh, M.; Zhang, X.; Kloc, C.; Tan, P. H.; Eda, G. Lattice Dynamics in Mono- and Few-Layer Sheets of WS_2 and WSe_2. *Nanoscale* **2013**, *5*, 9677−9683.
(30) Wang, H.; Bang, J.; Sun, Y.; Liang, L.; West, D.; Meunier, V.; Zhang, S. The Role of Collective Motion in the Ultrafast Charge Transfer in Van Der Waals Heterostructures. *Nat. Commun.* **2016**, *7*, 1−9.
(31) Parandekar, P. V.; Tully, J. C. Detailed Balance in Ehrenfest Mixed Quantum-Classical Dynamics. *J. Chem. Theory Comput.* **2006**, *2*, 229−235.
(32) Jain, A.; Subotnik, J. E. Vibrational Energy Relaxation: A Benchmark for Mixed Quantum-Classical Methods. *J. Phys. Chem. A* **2018**, *122*, 16−27.
(33) Prezhdo, O. V. Mean Field Approximation for the Stochastic Schrödinger Equation. *J. Chem. Phys.* **1999**, *111*, 8366−8377.
(34) Akimov, A. V.; Long, R.; Prezhdo, O. V. Coherence Penalty Functional: A Simple Method for Adding Decoherence in Ehrenfest Dynamics. *J. Chem. Phys.* **2014**, *140*, 194107.
(35) Esch, M. P.; Levine, B. G. Decoherence-Corrected Ehrenfest Molecular Dynamics on Many Electronic States. *J. Chem. Phys.* **2020**, *153*, 114104.

https://doi.org/10.1021/acs.nanolett.1c01083
Nano Lett. 2021, 21, 4403−4409